Research Square

Preprints are preliminary reports that have not undergone peer review.
They should not be considered conclusive, used to inform clinical practice,
or referenced by the media as validated information.

On the motion of a catamaran-type wave energy converter under periodic external forcing

Xinhang Li
Fudan University
Zhijie Cai
zhijiecai@163.com

Fudan University

Research Article

Keywords:

Posted Date: November 2nd, 2026

DOI: https://doi.org/10.21203/rs.3.rs-11251249/v1

License: This work is licensed under a Creative Commons Attribution 4.0 International License.
Read Full License

Additional Declarations: No competing interests reported.

On the motion of a catamaran-type wave energy converter under periodic external forcing

Xinhang Li[1] and Zhijie Cai[1,2,3*]

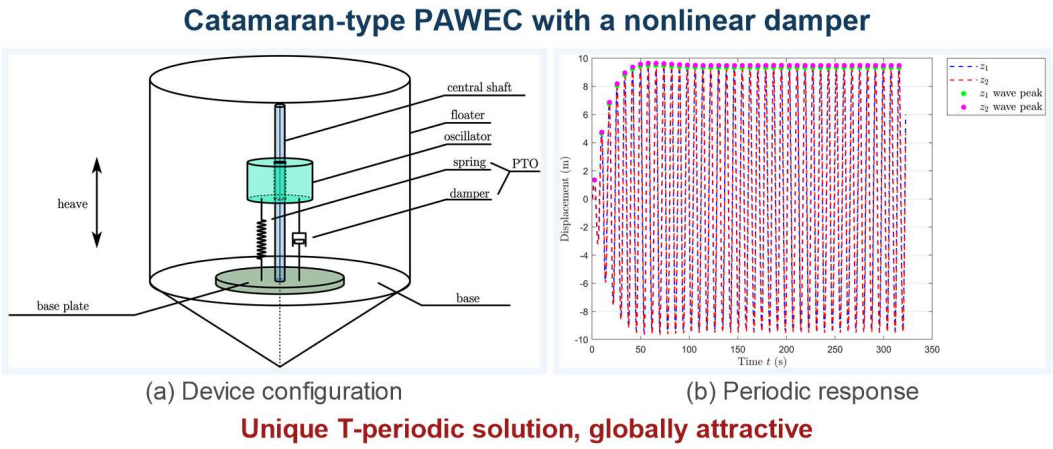
[1]School of Mathematical Sciences, Fudan University, Shanghai 200433, China.
[2]Shanghai Key Laboratory of Contemporary Applied Mathematics, Shanghai 200433, China.
[3]Key Laboratory of Nonlinear Mathematical Models and Methods of Ministry of Education, Shanghai 200433, China.

*Corresponding author(s). E-mail(s): zhijiecai@163.com;
Contributing authors: 24110180028@m.fudan.edu.cn;

Abstract

Wave energy is one of the most promising renewable energy sources, and the catamaran-type point-absorption wave energy converter (PAWEC) is a widely studied prototype because of its compact size and its ability to absorb wave energy from all directions. The dynamics of such a device, however, are described by a system of high-dimensional nonlinear non-autonomous vibration equations under $\boldsymbol{T}$-periodic excitation, and whether the system possesses a stable periodic response has not been rigorously established in general. In this paper, the radiation damping is represented by an equivalent constant-coefficient linear damping model commonly used in engineering practice, and the PTO system is modeled as a linear spring acting in parallel with a nonlinear damper whose damping coefficient is proportional to a power of the relative velocity. Using the coincidence degree theory of Mawhin, we prove that the resulting system admits a unique $\boldsymbol{T}$-periodic solution, and we further prove that the solution of the Cauchy problem with arbitrary initial values converges asymptotically to this periodic solution. Numerical simulations for a catamaran-type PAWEC confirm the theoretical results and illustrate the global attractivity of the periodic response.

Keywords: wave energy converter (WEC); periodic forcing; coincidence degree theory; nonlinear damping; ordinary differential equations (ODEs)



Graphical Abstract

1 Introduction

With the rapid development of socio-economic and science and technology, global energy consumption has been increasing rapidly. Traditional energy sources, such as coal, oil, and natural gas, have limited reserves, and they cause severe environmental pollution during the process of developing and utilizing. Consequently, the exploitation and application of clean and renewable energy sources are of great significance. Due to its vast reserves, wave energy is one of the vital renewable energy sources, which plays a key role in the global renewable energy layout [1]. The wave energy flux per unit area can reach 2∼3 kW/m^2, which is significantly higher than that of solar energy (0.1∼0.3 kW/m^2) and wind energy (0.5 kW/m^2) [2, 3]. However, the waves have stochasticity and vary greatly across multiple time scales of wave energy, making it one of the most difficult marine energy sources to capture [4, 5].

Wave energy converter (WEC) is the core technology of wave power generation. WEC is primarily classified into three categories based on the principle of energy capture: oscillating buoy type, oscillating water column type, and overtopping type. The oscillating buoy type WEC utilizes wave-induced motions of a floater to drive the Power Take-Off (PTO) system for energy conversion. The oscillating water column type WEC utilizes waves to force the water column within an air chamber to move, compressing air to drive the turbine generator. The overtopping type WEC guides waves over the weir crest into an elevated reservoir, utilizing the difference of hydraulic head to generate electricity [4]. The oscillating body WEC can be further divided into point-absorption, attenuators, and terminators. The point-absorption type wave energy converter (PAWEC) has dimensions smaller than the incident wavelength and can capture wave energy from all directions, making it one of the most widely studied prototypes. The attenuator type WEC has its long axes parallel to the direction of wave propagation. The terminator type WEC has its primary axes perpendicular to the wave direction, with dimensions similar to or larger than the incident wavelength [4, 6, 7]. Furthermore, WEC can be categorized by its deployment method into fixed

and floating types. Fixed WEC is anchored on the seabed or breakwaters, and is predominantly installed in nearshore shallow waters. Floating WEC, typically anchored to the seabed through a mooring system, is suitable for deep-water, and has become the current mainstream choice for deep-sea wave energy development [4, 6, 8].

This paper focuses on the PAWEC. A typical PAWEC, especially the point-absorption type, generally comprises several key subsystems: one or more capture floaters, a PTO system integrated with a power generation unit, and a control system [9–11]. In this configuration, the floaters serve as the energy harvesting components to capture wave energy, while the control system optimizes the efficiency of energy extraction. Subsequently, the PTO system converts the captured energy into certain form of mechanical or electrical energy.

At present, the mainstream analytical methods for PAWEC dynamics include the linear frequency domain method, the linear/weakly nonlinear time domain method, the computational fluid dynamics (CFD), and hybrid methods. The linear frequency domain method, based on the linear potential flow theory, solves the steady state periodic response of the system in the frequency domain. It is characterized by high computational efficiency and is suitable for preliminary design and parameter scanning; however, it cannot handle nonlinear problems. Some software, such as AQWA, WAMIT, etc., is commonly used for numerical simulations [8, 12]. The linear/weakly nonlinear time domain method, based on the Cummins equation, transforms frequency domain hydrodynamic coefficients into the time domain [7, 13]. The time-domain equations of this method can be solved by standard ODE solvers, e.g., the Runge-Kutta method (MATLAB ode45), as in simulation tools such as WEC-Sim. The convolution term (fluid memory effect) corresponding to radiation damping in the Cummins equation introduces a dependency on motion history, making it impossible to directly use classical constant coefficient linear ODE methods. Existing research generally adopts two approaches: One involves linearization under the assumption of single-frequency wave excitation to obtain the steady state response of the device [14–16]; the other introduces equivalent control equations to replace the radiation damping term [13, 17]. The CFD methods, by solving the Navier-Stokes equations using computational software such as ANSYS Fluent and OpenFOAM, can simulate strong nonlinear phenomena, such as viscosity, vortex flow, breaking waves, etc., more accurately. However, it has extremely high computational costs and is usually used for key component verification or specific phenomenon research. The hybrid method adopts a mixed modeling framework combining frequency domain BEM, time domain multi-body dynamics, and local CFD corrections, which also has high computational costs [3].

The dynamic analysis of wave energy converter (WEC) encounters numerous challenges. The real ocean environment exhibits strong nonlinearities, including viscous damping (especially for non-streamlined or small-sized floaters), vortex-induced vibration, nonlinear restoring forces induced by large-amplitude motion, PTO nonlinearities (e.g., Coulomb friction, dead zone), and mooring nonlinearities. Traditional linear potential flow theory often underestimates these effects, leading to overprediction of power capture and inaccurate motion responses [3]. For catamaran-type or multi-body WEC, the hydrodynamic coupling (radiation, diffraction) between floaters is

exceedingly complex. Meanwhile, practical devices often exhibit coupled motions with multiple degrees of freedom [18]. Furthermore, simulating the response and structural loads of devices under extreme conditions, such as once-in-a-century storms, demands high robustness of the models and algorithms.

To show that a catamaran-type PAWEC device exhibits steady state periodic motion under nonlinear PTO conditions, this paper employs a constant coefficient linear damping model, commonly used in engineering, to equivalently represent the radiation damping effect [9, 14]. Using the linear/weakly nonlinear time domain method, the existence and uniqueness of the periodic solutions of the system are proved, providing a theoretical basis for the rationality of the steady state periodic response.

The catamaran-type PAWEC is illustrated in Fig. 1. The surface floater is a

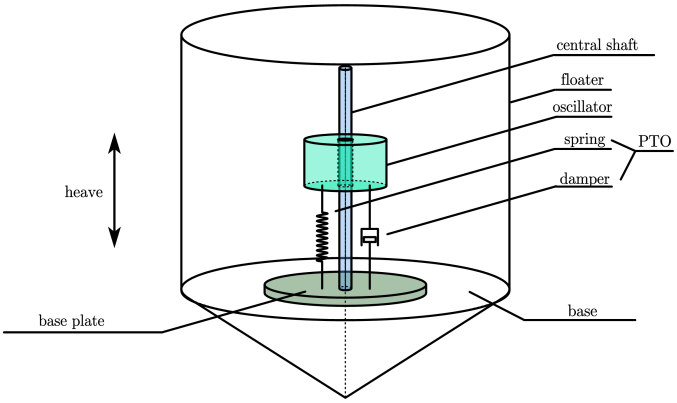


Fig. 1 Catamaran-type PAWEC diagram[19]

cylindrical-conical body, which is connected to an internal oscillator via the PTO system [9]. This oscillator is sleeved over the central shaft of the floater and is constrained to move vertically along the shaft. The PTO system consists of a linear spring and a nonlinear damper.

Under wave excitation, the surface floater undergoes heave motion, which in turn induces heave motion of the internal oscillator through the PTO system. The relative velocity between the floater and the oscillator converts mechanical energy into electrical energy via the damping mechanism within the PTO.

The geometric parameters of the floater and the oscillator are illustrated in Fig. 2. The variables z_1 and z_2 denote the vertical displacements of the centers of mass of the floater and the oscillator relative to their equilibrium positions, respectively. h_1 represents the height of the conical part of the floater, and r is the radius of the floater base. h_2 denotes the vertical distance from the floater's center of mass to the tip of the cone. h_3 represents the height of the oscillator. h_4 is the height of the cylinder part of the floater.

We consider the nonlinear damper whose damping coefficient is proportional to a power of the absolute relative velocity between the floater and the oscillator. The

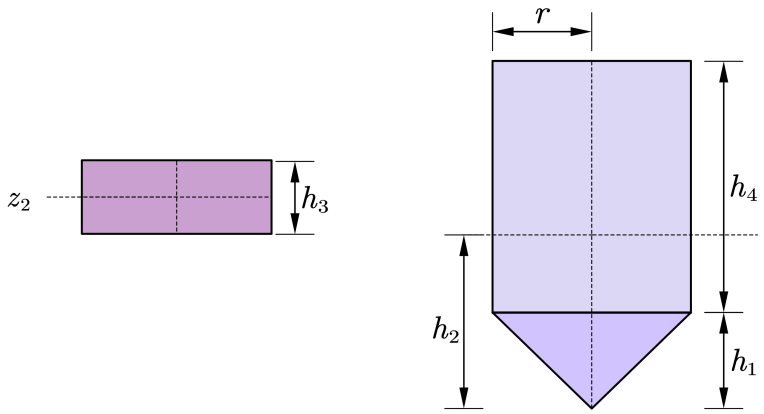


Fig. 2 The shapes and geometric parameters of the floater and oscillator

damping force is given by

$$c\left|\frac{\mathrm{d}z_1}{\mathrm{d}t}-\frac{\mathrm{d}z_2}{\mathrm{d}t}\right|^{\alpha}\left(\frac{\mathrm{d}z_1}{\mathrm{d}t}-\frac{\mathrm{d}z_2}{\mathrm{d}t}\right),$$

where $c>0$, and $\alpha\in(0,1]$.

The forces acting on the floater are listed below:

(1) Radiation damping force generated by the waves, where C_a denotes the equivalent damping coefficient, assumed constant for simplicity;

(2) Wave excitation force $f_e\cos(\omega t)$ produced by periodic small amplitude waves, where $f_e>0$ is the amplitude, ω is the angular frequency, corresponding to the period $T=2\pi/\omega$;

(3) Hydrostatic restoring force $-k_f z_1$, where the coefficient $k_f=\rho g S$ is proportional to the cross-sectional area of the floater immersed at the water surface $S=\pi r^2$, and ρ denotes the water density;

(4) Damping force from the nonlinear damper;

(5) Spring force $-k_s(z_1-z_2)$, where k_s denotes the spring coefficient.

By Newton's second law of motion,

$$\begin{aligned}(m_a+m_f)\frac{\mathrm{d}^2z_1}{\mathrm{d}t^2}=&-C_a\frac{\mathrm{d}z_1}{\mathrm{d}t}-k_f z_1-c\left|\frac{\mathrm{d}z_1}{\mathrm{d}t}-\frac{\mathrm{d}z_2}{\mathrm{d}t}\right|^{\alpha}\left(\frac{\mathrm{d}z_1}{\mathrm{d}t}-\frac{\mathrm{d}z_2}{\mathrm{d}t}\right)\\&-k_s\left(z_1-z_2\right)+f_e\cos(\omega t),\end{aligned}\tag{1.1}$$

where m_f denotes the mass of the floater, m_a signifies the added mass generated by the fluid surrounding the floater.

The forces acting on the oscillator are listed below:

(1) Damping force;

(2) Spring force.

By Newton's second law of motion,

$$m_v\frac{\mathrm{d}^2z_2}{\mathrm{d}t^2}=c\left|\frac{\mathrm{d}z_1}{\mathrm{d}t}-\frac{\mathrm{d}z_2}{\mathrm{d}t}\right|^{\alpha}\left(\frac{\mathrm{d}z_1}{\mathrm{d}t}-\frac{\mathrm{d}z_2}{\mathrm{d}t}\right)+k_s\left(z_1-z_2\right).\tag{1.2}$$

where m_v represents the mass of the oscillator.

Equations (1.1)–(1.2) constitute the system of equations of motion of the PAWEC. This system is further reduced to a first-order form expressed as

$$\frac{\mathrm{d}\boldsymbol{x}}{\mathrm{d}t} = \boldsymbol{A}\boldsymbol{x} + \boldsymbol{g}(\boldsymbol{x}) + \boldsymbol{f}(t), \tag{1.3}$$

where $\boldsymbol{x} = (z_1, z_2, v_1, v_2)^{\mathrm{T}}$,

$$\boldsymbol{A} = \begin{pmatrix} 0 & 0 & 1 & 0 \\ 0 & 0 & 0 & 1 \\ -\dfrac{k_s + k_f}{m_f + m_a} & \dfrac{k_s}{m_f + m_a} & -\dfrac{C_a}{m_f + m_a} & 0 \\ \dfrac{k_s}{m_v} & -\dfrac{k_s}{m_v} & 0 & 0 \end{pmatrix}, \tag{1.4}$$

$$\boldsymbol{g}(\boldsymbol{x}) = \begin{pmatrix} 0 \\ 0 \\ -\dfrac{c|v_1 - v_2|^{\alpha}(v_1 - v_2)}{m_f + m_a} \\ \dfrac{c|v_1 - v_2|^{\alpha}(v_1 - v_2)}{m_v} \end{pmatrix}, \tag{1.5}$$

$$\boldsymbol{f}(t) = \begin{pmatrix} 0 \\ 0 \\ \dfrac{f_e \cos(\omega t)}{m_f + m_a} \\ 0 \end{pmatrix}. \tag{1.6}$$

While the mathematical characterization of catamaran-type wave energy models is relatively mature [20], analytical research into their nonlinear dynamics remains insufficient. Existing analyses are predominantly based on linear or weakly nonlinear assumptions. When a system can be simplified into a linear time-invariant system under regular wave excitation of a single frequency, its steady state response is necessarily a periodic solution of the same frequency. The amplitude and phase of such solutions can be directly obtained via frequency domain algebraic equations or time domain integration; this serves as the mathematical foundation for Response Amplitude Operator analysis [3, 6]. If system parameters exhibit periodic variations, the system reduces to a linear periodic coefficient system. In such cases, the existence and stability of periodic solutions can be numerically determined using Floquet theory, specifically by analyzing the eigenvalues of the state transition matrix [21].

The analytical approaches used for these linearized models provide an essential reference for investigating nonlinear systems. For weakly nonlinear systems, a linear periodic solution is typically adopted as the zeroth-order approximation, with perturbation methods employed to derive nonlinear corrections. The method of multiple scales can be extended to handle forced vibration systems with strong nonlinear damping, revealing their periodic solutions and stability characteristics [21, 22]. However, when system responses exhibit subharmonics, period-doubling components, or

significant deviations from linear resonance predictions, this indicates that nonlinear mechanisms that are not captured by linearization have become dominant. In such cases, theoretical tools from nonlinear dynamics are required to investigate the existence, multiplicity, and bifurcation behavior of periodic solutions [23].

Although numerical methods can provide approximate estimations of the frequency-amplitude relationships in nonlinear systems [24], a rigorous proof for the existence of steady state periodic solutions in catamaran-type WEC, particularly under complex mechanisms such as nonlinear PTO, remains a significant theoretical gap. Addressing this gap will establish a solid mathematical foundation for the dynamical design, stability analysis, and performance optimization of nonlinear WEC systems.

This paper analyzes the dynamical equations (1.3) of a catamaran-type PAWEC device equipped with a nonlinear damper. Utilizing coincidence degree theory, the existence, uniqueness, and global attractivity of periodic solutions under single-frequency sinusoidal wave excitation are proved. These analytical results are further validated by numerical simulations.

The remainder of this paper is organized as follows: Section 2 provides a rigorous proof for the existence of periodic solutions corresponding to the excitation frequency based on coincidence degree theory. Section 3 proves the global attractivity of periodic solutions using Lyapunov stability theory. Section 4 demonstrates the uniqueness of the periodic solution to the system. Section 5 verifies the qualitative analysis results through numerical simulations; Section 6 concludes the paper and provides an outlook for future work.

2 Existence of T-Periodic Solutions

To obtain the existence of periodic solutions to system (1.3), the following definitions are introduced.

Definition 1 [25] Suppose that $\Omega \subset \mathbb{R}^n$ is a Lebesgue measurable set with positive measure. If a function $\boldsymbol{h}(\boldsymbol{x}, u) : \Omega \times \mathbb{R} \to \mathbb{R}^n$ satisfies

(1) For every $u \in \mathbb{R}$, the mapping $\boldsymbol{x} \mapsto \boldsymbol{h}(\boldsymbol{x}, u)$ is a measurable function.

(2) For almost every $\boldsymbol{x} \in \Omega$, the mapping $u \mapsto \boldsymbol{h}(\boldsymbol{x}, u)$ is a continuous function.

Then $\boldsymbol{h}$ is called a Carathéodory function.

Definition 2 [23] Suppose that X and Z are two real normed linear spaces, and $L : D(L) \subset X \to Z$ is a Fredholm linear mapping of index zero. Let Ω be a bounded open set in X, $N : \overline{\Omega} \to Z$ be L-compact, and $F : D(L) \cap \overline{\Omega} \to Z$ be a mapping of the form $F = L + N$ such that $0 \notin F(D(L) \cap \partial\Omega)$. Denote by C_L the set of all pairs (F, Ω). The mapping $D_L : C_L \mapsto \mathbb{Z}$ is called the coincidence degree with respect to L, if $D_L \not\equiv 0$ and satisfies the following two properties:

(1) **Additivity-Excision Property**

If $(F, \Omega) \in C_L$ and Ω_1, Ω_2 are disjoint open subsets of Ω such that

$$0 \notin F[D(L) \cap (\overline{\Omega} \setminus (\Omega_1 \cup \Omega_2))],$$

then (F, Ω_1) and (F, Ω_2) belong to C_L, and

$$D_L(F, \Omega) = D_L(F, \Omega_1) + D_L(F, \Omega_2).$$

(2) **Homotopy Invariance**

Let Γ be an open bounded subset of $X \times [0,1]$, and the mapping $\mathcal{H} : (D(L) \times [0,1]) \cap \overline{\Gamma} \to Z$ be

$$\mathcal{H}(x,\lambda) = Lx + \mathcal{N}(x,\lambda),$$

where $\mathcal{N} : \overline{\Gamma} \to Z$ is L-compact on $\overline{\Gamma}$. Furthermore, $\forall \lambda \in [0,1]$, $x \in D(L) \cap (\partial\Gamma)_\lambda$, $\mathcal{H}(x,\lambda) \neq 0$, where $(\partial\Gamma)_\lambda = \{x \in X : (x,\lambda) \in \partial\Gamma\}$. Then, the mapping $\lambda \mapsto D_L(\mathcal{H}(\cdot,\lambda),\Gamma_\lambda)$ is constant in $[0,1]$, where $\Gamma_\lambda = \{x \in X \mid (x,\lambda) \in \Gamma\}$.

Consider the following periodic boundary value problem

$$\frac{\mathrm{d}\boldsymbol{x}}{\mathrm{d}t} = \boldsymbol{u}(\boldsymbol{x},t), \tag{2.1}$$

$$\boldsymbol{x}(0) = \boldsymbol{x}(T), \tag{2.2}$$

where $\boldsymbol{u} : [0,T] \times \mathbb{R}^n \to \mathbb{R}^n$ is a Carathéodory function with $T > 0$.

To analyze system (2.1)–(2.2), a family of homotopy equations is constructed as

$$\frac{\mathrm{d}\boldsymbol{x}}{\mathrm{d}t} = \boldsymbol{w}(\boldsymbol{x},t;\lambda), \quad \lambda \in [0,1], \tag{2.3}$$

where for any given $\lambda \in [0,1]$, $\boldsymbol{w}(\boldsymbol{x},t;\lambda) : [0,T] \times \mathbb{R}^n \times [0,1] \to \mathbb{R}^n$ is a Carathéodory function satisfying

$$\boldsymbol{w}(\boldsymbol{x},t;1) = \boldsymbol{u}(\boldsymbol{x},t), \tag{2.4}$$

$$\boldsymbol{w}(\boldsymbol{x},t;0) = \boldsymbol{v}(\boldsymbol{x}). \tag{2.5}$$

We have the following lemma on the existence of solution to (2.1)–(2.2).

Lemma 1 [23] Let G be an open bounded subset of $\mathbb{R}^n$ such that

(1) For any given $\lambda \in [0,1)$, if the solution $\boldsymbol{x}$ to system (2.3) with initial data (2.2) satisfies

$$\boldsymbol{x}(t) \in \overline{G}, \quad \forall t \in [0,T],$$

then

$$\boldsymbol{x}(t) \in G, \quad \forall t \in [0,T].$$

(2) The coincidence degree of $\boldsymbol{v}$ $(= \boldsymbol{w}(\boldsymbol{x},t;0)$, see (2.5)) in G

$$\deg(\boldsymbol{v},G) \neq 0. \tag{2.6}$$

Then, there is at least one solution $\boldsymbol{x}$ to system (2.1)–(2.2), such that $\boldsymbol{x}(t) \in \overline{G}$, $\forall t \in [0,T]$.

Next, we discuss the existence of periodic solutions to system (1.3). Throughout the paper, we assume that

$$m_f + m_a > 0, \quad m_v > 0, \quad C_a > 0, \quad c > 0, \quad k_s > 0, \quad k_f > 0, \quad \alpha \in (0,1],$$

which holds for the physical parameters used in Section 5. Take $X = Z = C_T$, where

$$C_T = \{\boldsymbol{x} \in C^0([0,T];\mathbb{R}^n) \mid \boldsymbol{x}(0) = \boldsymbol{x}(T)\}$$

carries the supremum norm, and let $L = \dfrac{\mathrm{d}}{\mathrm{d}t}$ be defined on $D(L) = X \cap C^1([0,T];\mathbb{R}^n)$. Then $\ker L \cong \mathbb{R}^n$ consists of the constant functions and $\operatorname{Im} L = \{u \in C_T \mid \displaystyle\int_0^T u(t)\,\mathrm{d}t = 0\}$, so L is a Fredholm operator of index zero. Since $K_P := (L|_{D(L)\cap\ker P})^{-1}$ is an integral operator, it is compact by the Arzelà–Ascoli theorem; hence every continuous operator N mapping bounded subsets of X into bounded subsets of Z is L-compact. This applies to the operator N induced by the right-hand side of (1.3), because $\boldsymbol{g}$ and $\boldsymbol{f}$ are continuous and bounded on bounded sets. Write $\deg(F,\Omega) = D_L(F,\Omega)$.

Theorem 1 System (1.3) admits a T-periodic solution with $T = \dfrac{2\pi}{\omega}$.

Proof Construct a family of homotopy equations

$$\frac{\mathrm{d}\boldsymbol{x}}{\mathrm{d}t} = \boldsymbol{A}\boldsymbol{x} + \boldsymbol{g}(\boldsymbol{x}) + \lambda \boldsymbol{f}(t), \quad \lambda \in [0,1], \tag{2.7}$$

where $\boldsymbol{x} = (z_1, z_2, v_1, v_2)^{\mathrm{T}}$.

When $\lambda = 1$, system (2.7) is just the system (1.3). When $\lambda = 0$, system (2.7) reduces to an autonomous system

$$\frac{\mathrm{d}\boldsymbol{x}}{\mathrm{d}t} = \boldsymbol{A}\boldsymbol{x} + \boldsymbol{g}(\boldsymbol{x}). \tag{2.8}$$

By (1.4)–(1.5), $\mathbf{0}$ is the unique equilibrium of (2.8): at an equilibrium the first two equations give $v_1 = v_2 = 0$, the fourth gives $k_s(z_1 - z_2) = 0$, and then the third gives $k_f z_1 = 0$, so that $z_1 = z_2 = 0$.

Construct a Lyapunov function

$$V(\boldsymbol{x}) = \frac{1}{2}(m_f + m_a)v_1^2 + \frac{1}{2}m_v v_2^2 + \frac{1}{2}k_f z_1^2 + \frac{1}{2}k_s(z_1 - z_2)^2. \tag{2.9}$$

V is a positive-definite function.

When $\lambda = 0$, the total derivative of V along the phase orbit of the autonomous system (2.8) is

$$\frac{\mathrm{d}V}{\mathrm{d}t} = -C_a v_1^2 - c|v_1 - v_2|^{\alpha}(v_1 - v_2)^2 \le 0. \tag{2.10}$$

Thus V is non-increasing along the orbits of the autonomous system (2.8).

Denote

$$\boldsymbol{v}(\boldsymbol{x}) = \boldsymbol{A}\boldsymbol{x} + \boldsymbol{g}(\boldsymbol{x}). \tag{2.11}$$

Since $\boldsymbol{g}$ depends on $\boldsymbol{x}$ only through $v_1 - v_2$, and since $\alpha > 0$ implies $\boldsymbol{g}(\boldsymbol{x}) = o(|\boldsymbol{x}|)$ as $\boldsymbol{x} \to \mathbf{0}$, the Jacobian of $\boldsymbol{v}$ at $\mathbf{0}$ is $\boldsymbol{A}$, so that $\det\left(\partial\boldsymbol{v}/\partial\boldsymbol{x}|_{\boldsymbol{x}=\mathbf{0}}\right) = \det\boldsymbol{A} = \dfrac{k_s k_f}{(m_f + m_a)m_v} > 0$; moreover, $\mathbf{0}$ is the only zero of $\boldsymbol{v}$. By the standard index formula for a nondegenerate zero (see, e.g., [26]), for every bounded open set $G_0 \subset \mathbb{R}^4$ containing

$\mathbf{0}$ with $\mathbf{0} \notin \boldsymbol{v}(\partial G_0)$ one has

$$\deg(\boldsymbol{v}, G_0) = \operatorname{sign}\left(\det\left(\frac{\partial \boldsymbol{v}}{\partial \boldsymbol{x}}\Big|_{\boldsymbol{x}=\mathbf{0}}\right)\right) = 1,$$

in particular $\deg(\boldsymbol{v}, G) = 1$ for the bounded open set G constructed below. Hence (2.6) holds.

The verification of condition (1) in Lemma 1 is divided into three steps.

Step 1 $\|v_1\|_{L^2([0,T])}$ and $\|v_2\|_{L^2([0,T])}$ are uniformly bounded.

The total derivative of V along the phase orbit of system (2.7) is

$$\frac{\mathrm{d}V}{\mathrm{d}t} = -C_a v_1^2 - c|v_1 - v_2|^{\alpha+2} + \lambda f_e v_1 \cos(\omega t). \tag{2.12}$$

For any $\lambda \in [0,1]$ and any T-periodic solution $\boldsymbol{x}(t)$ to system (2.7), we have

$$\begin{aligned} 0 &= \int_0^T \frac{\mathrm{d}V}{\mathrm{d}t}(\boldsymbol{x}(t))\mathrm{d}t \\ &= -C_a \int_0^T v_1^2(t)\mathrm{d}t - c\int_0^T |v_1(t) - v_2(t)|^{\alpha+2}\mathrm{d}t + \int_0^T \lambda f_e v_1(t)\cos(\omega t)\mathrm{d}t. \end{aligned} \tag{2.13}$$

Applying the Cauchy-Schwarz inequality,

$$C_a\|v_1\|^2_{L^2([0,T])} + c\|v_1 - v_2\|^{\alpha+2}_{L^{\alpha+2}([0,T])} \le f_e\left(\frac{T}{2}\right)^{1/2}\|v_1\|_{L^2([0,T])}. \tag{2.14}$$

Hence,

$$\|v_1\|_{L^2([0,T])} \le \frac{f_e}{C_a}\left(\frac{T}{2}\right)^{1/2}. \tag{2.15}$$

Substituting (2.15) into (2.14), we have

$$c\|v_1 - v_2\|^{\alpha+2}_{L^{\alpha+2}([0,T])} \le \frac{f_e^2}{C_a}\frac{T}{2}. \tag{2.16}$$

Due to the embedding theorem in L^p spaces [27]

$$\|x\|_{L^2([0,T])} \le T^{\frac{\alpha}{2(\alpha+2)}}\|x\|_{L^{\alpha+2}([0,T])},$$

it follows that

$$\begin{aligned} \|v_2\|_{L^2([0,T])} &\le \|v_2 - v_1\|_{L^2([0,T])} + \|v_1\|_{L^2([0,T])} \\ &\le T^{\frac{\alpha}{2(\alpha+2)}}\|v_2 - v_1\|_{L^{\alpha+2}([0,T])} + \|v_1\|_{L^2([0,T])} \\ &\le \left(\frac{f_e^2}{2cC_a}\right)^{\frac{1}{\alpha+2}} T^{\frac{1}{2}} + \frac{f_e}{\sqrt{2}C_a}T^{\frac{1}{2}}. \end{aligned} \tag{2.17}$$

Step 2 $\|z_1\|_{L^\infty([0,T])}$ and $\|z_2\|_{L^\infty([0,T])}$ are uniformly bounded.

From the third and fourth equations of system (2.7),

$$(m_f + m_a)\frac{\mathrm{d}v_1}{\mathrm{d}t} + m_v\frac{\mathrm{d}v_2}{\mathrm{d}t} = -C_a v_1 - k_f z_1 + \lambda f_e \cos(\omega t). \tag{2.18}$$

By integrating both sides with respect to t over $[0, T]$, and noting that $v_1 = \dfrac{\mathrm{d}z_1}{\mathrm{d}t}$, we have $\displaystyle\int_0^T z_1(t)\mathrm{d}t = 0$. By using the mean value theorem for integrals, there exists $t_0 \in [0, T]$ such that $z_1(t_0) = 0$.

Integrating the first equation of system (2.7) from t_0 to t,

$$z_1(t) = z_1(t_0) + \int_{t_0}^t v_1(\tau)\mathrm{d}\tau = \int_{t_0}^t v_1(\tau)\mathrm{d}\tau, \tag{2.19}$$

thus

$$\begin{aligned} |z_1(t)| &\le \int_{t_0}^t |v_1(\tau)|\mathrm{d}\tau \le |t - t_0|^{\frac{1}{2}}\|v_1\|_{L^2([0,T])} \\ &\le |t - t_0|^{\frac{1}{2}}\frac{f_e}{C_a}\left(\frac{T}{2}\right)^{1/2} \le \frac{f_e}{\sqrt{2}C_a}T. \end{aligned} \tag{2.20}$$

Integrating the fourth equation of system (2.7) from 0 to T,

$$-c\int_0^T |v_1(t) - v_2(t)|^\alpha (v_1(t) - v_2(t))\mathrm{d}t - k_s\int_0^T (z_1(t) - z_2(t))\mathrm{d}t = 0, \tag{2.21}$$

which leads to

$$k_s\left|\int_0^T (z_1(t) - z_2(t))\mathrm{d}t\right| \le c\|v_1(t) - v_2(t)\|^{\alpha+1}_{L^{\alpha+1}([0,T])}. \tag{2.22}$$

By using the embedding theorem in L^p spaces

$$\|x\|_{L^{\alpha+1}([0,T])} \le T^{\frac{1}{(\alpha+1)(\alpha+2)}}\|x\|_{L^{\alpha+2}([0,T])},$$

and combining with (2.16), we can obtain

$$k_s\left|\int_0^T (z_1(t) - z_2(t))\mathrm{d}t\right| \le \left(c^{\frac{1}{\alpha+1}}\frac{f_e^2}{2C_a}\right)^{\frac{\alpha+1}{\alpha+2}}T. \tag{2.23}$$

By the mean value theorem for integrals, there exists $t_1 \in [0, T]$ such that

$$|z_1(t_1) - z_2(t_1)| \le \frac{1}{k_s}\left(c^{\frac{1}{\alpha+1}}\frac{f_e^2}{2C_a}\right)^{\frac{\alpha+1}{\alpha+2}}.$$

Thus

$$\begin{aligned} |z_2(t_1)| &\le |z_1(t_1) - z_2(t_1)| + |z_1(t_1)| \\ &\le \frac{1}{k_s}\left(c^{\frac{1}{\alpha+1}}\frac{f_e^2}{2C_a}\right)^{\frac{\alpha+1}{\alpha+2}} + |t_1 - t_0|^{\frac{1}{2}}\frac{f_e}{C_a}\left(\frac{T}{2}\right)^{1/2} \end{aligned}$$

$$\leq \frac{1}{k_s}\left(c^{\frac{1}{\alpha+1}}\frac{f_e^2}{2C_a}\right)^{\frac{\alpha+1}{\alpha+2}} + \frac{f_e}{\sqrt{2}C_a}T. \tag{2.24}$$

Similarly, from the second equation of system (2.7), we have

$$z_2(t) = z_2(t_1) + \int_{t_1}^{t} v_2(\tau)\mathrm{d}\tau, \tag{2.25}$$

thus

$$\begin{aligned}
|z_2(t)| &\leq |z_2(t_1)| + \int_{t_1}^{t} |v_2(\tau)|\mathrm{d}\tau \\
&\leq |z_2(t_1)| + |t-t_1|^{\frac{1}{2}}\|v_2\|_{L^2([0,T])} \\
&\leq \frac{1}{k_s}\left(c^{\frac{1}{\alpha+1}}\frac{f_e^2}{2C_a}\right)^{\frac{\alpha+1}{\alpha+2}} + \frac{f_e}{\sqrt{2}C_a}T + |t-t_1|^{\frac{1}{2}}\left[\frac{f_e}{\sqrt{2}C_a} + \left(\frac{f_e^2}{2cC_a}\right)^{\frac{1}{\alpha+2}}\right]T^{\frac{1}{2}} \\
&\leq \frac{1}{k_s}\left(c^{\frac{1}{\alpha+1}}\frac{f_e^2}{2C_a}\right)^{\frac{\alpha+1}{\alpha+2}} + \left[\frac{\sqrt{2}f_e}{C_a} + \left(\frac{f_e^2}{2cC_a}\right)^{\frac{1}{\alpha+2}}\right]T.
\end{aligned} \tag{2.26}$$

Step 3 $\|v_1(t)\|_{L^\infty([0,T])}$ and $\|v_2(t)\|_{L^\infty([0,T])}$ are uniformly bounded.

Since $\boldsymbol{x}(t)$ is a periodic solution, by Rolle's theorem, there exist $t_2, t_3 \in [0,T]$ such that $v_1(t_2) = v_2(t_3) = 0$.

Integrating the third equation of system (2.7) from t_2 to t yields

$$\begin{aligned}
\int_{t_2}^{t}\frac{\mathrm{d}v_1}{\mathrm{d}t}(\tau)\mathrm{d}\tau = \frac{1}{m_f+m_a}\Bigg[&-c\int_{t_2}^{t}|v_1-v_2|^{\alpha}(v_1-v_2)\mathrm{d}\tau - C_a\int_{t_2}^{t}v_1\mathrm{d}\tau \\
&-k_s\int_{t_2}^{t}(z_1-z_2)\mathrm{d}\tau - k_f\int_{t_2}^{t}z_1\mathrm{d}\tau + \lambda f_e\int_{t_2}^{t}\cos(\omega\tau)\mathrm{d}\tau\Bigg].
\end{aligned} \tag{2.27}$$

Applying the Cauchy-Schwarz inequality, we have

$$\begin{aligned}
|v_1(t)| &\leq \frac{1}{m_f+m_a}\Big[c\|v_1-v_2\|^{\alpha+1}_{L^{\alpha+1}([0,T])} + 2C_a\|z_1\|_{L^\infty([0,T])} \\
&\quad + k_sT(\|z_1\|_{L^\infty([0,T])} + \|z_2\|_{L^\infty([0,T])}) + k_fT\|z_1\|_{L^\infty([0,T])} + \frac{2}{\omega}f_e\Big] \\
&\leq \frac{1}{m_f+m_a}\Bigg[\left(c^{\frac{1}{\alpha+1}}\frac{f_e^2}{2C_a}\right)^{\frac{\alpha+1}{\alpha+2}}T + \sqrt{2}f_eT + k_f\frac{f_e}{\sqrt{2}C_a}T^2 + \frac{2}{\omega}f_e \\
&\quad + k_s\left(\frac{1}{k_s}\left(c^{\frac{1}{\alpha+1}}\frac{f_e^2}{2C_a}\right)^{\frac{\alpha+1}{\alpha+2}}T + \left(\frac{3\sqrt{2}f_e}{2C_a} + \left(\frac{f_e^2}{2cC_a}\right)^{\frac{1}{\alpha+2}}\right)T^2\right)\Bigg] \\
&= \frac{1}{m_f+m_a}\Bigg[\frac{2}{\omega}f_e + 2\left(c^{\frac{1}{\alpha+1}}\frac{f_e^2}{2C_a}\right)^{\frac{\alpha+1}{\alpha+2}}T + \sqrt{2}f_eT \\
&\quad + \left(\frac{(3\sqrt{2}k_s+\sqrt{2}k_f)f_e}{2C_a} + k_s\left(\frac{f_e^2}{2cC_a}\right)^{\frac{1}{\alpha+2}}\right)T^2\Bigg].
\end{aligned} \tag{2.28}$$

Integrating the fourth equation of system (2.7) from t_3 to t, we have

$$\int_{t_3}^{t} \frac{\mathrm{d}v_2}{\mathrm{d}t}(\tau)\mathrm{d}\tau = \frac{1}{m_v}\left[-c\int_{t_3}^{t}|v_1-v_2|^{\alpha}(v_1-v_2)\mathrm{d}\tau - k_s\int_{t_3}^{t}(z_2-z_1)\mathrm{d}\tau\right]. \tag{2.29}$$

Also applying the Cauchy-Schwarz inequality, we obtain

$$\begin{aligned}
|v_2(t)| &\le \frac{1}{m_v}\left[c\|v_1-v_2\|^{\alpha+1}_{L^{\alpha+1}([0,T])} + k_sT\left(\|z_1\|_{L^{\infty}([0,T])}+\|z_2\|_{L^{\infty}([0,T])}\right)\right] \\
&\le \frac{1}{m_v}\left[\left(c^{\frac{1}{\alpha+1}}\frac{f_e^2}{2C_a}\right)^{\frac{\alpha+1}{\alpha+2}}T\right. \\
&\quad \left.+k_s\left(\frac{1}{k_s}\left(c^{\frac{1}{\alpha+1}}\frac{f_e^2}{2C_a}\right)^{\frac{\alpha+1}{\alpha+2}}T+\left(\frac{3\sqrt{2}f_e}{2C_a}+\left(\frac{f_e^2}{2cC_a}\right)^{\frac{1}{\alpha+2}}\right)T^2\right)\right] \\
&= \frac{1}{m_v}\left[\left(c^{\frac{1}{\alpha+1}}\frac{f_e^2}{2C_a}\right)^{\frac{\alpha+1}{\alpha+2}}T+k_s\left(\frac{3\sqrt{2}f_e}{2C_a}+\left(\frac{f_e^2}{2cC_a}\right)^{\frac{1}{\alpha+2}}\right)T^2\right].
\end{aligned} \tag{2.30}$$

Denote $R=\max\{z_1^{\max}, z_2^{\max}, v_1^{\max}, v_2^{\max}\}$, where $z_1^{\max}$, $z_2^{\max}$, $v_1^{\max}$, $v_2^{\max}$ are the upper bounds of the C^0 norms of z_1, z_2, v_1, v_2 obtained from (2.20), (2.26), (2.28), (2.30), respectively; here R serves only as a common numerical bound for the four components. Since these bounds are independent of λ, every T-periodic solution of system (2.7) satisfies $\|\boldsymbol{x}(t)\|_2 \le 2R$ for all $t\in[0,T]$. Therefore, taking $G=\mathbb{B}(0,2R+1)\subset\mathbb{R}^4$ yields $\boldsymbol{x}(t)\in G$, which verifies condition (1) in Lemma 1.

According to Lemma 1, system (1.3) admits a T-periodic solution. □

3 Global Attractivity of the T-Periodic Solution

Theorem 2 If $\boldsymbol{x}^*=(z_1^*,z_2^*,v_1^*,v_2^*)^{\mathrm{T}}$ is a T-periodic solution to system (1.3), then for any solution $\boldsymbol{x}=(z_1,z_2,v_1,v_2)^{\mathrm{T}}$ to system (1.3) with arbitrary initial data,

$$\begin{aligned}
&\lim_{t\to+\infty}|z_1(t)-z_1^*(t)|=0, \quad \lim_{t\to+\infty}|z_2(t)-z_2^*(t)|=0,\\
&\lim_{t\to+\infty}|v_1(t)-v_1^*(t)|=0, \quad \lim_{t\to+\infty}|v_2(t)-v_2^*(t)|=0.
\end{aligned}$$

Proof Let $\widetilde{\boldsymbol{x}}=\boldsymbol{x}-\boldsymbol{x}^*=(\widetilde{z}_1,\widetilde{z}_2,\widetilde{v}_1,\widetilde{v}_2)^{\mathrm{T}}$. Since $\boldsymbol{x}$ and $\boldsymbol{x}^*$ are two solutions to system (1.3), we can obtain

$$\frac{\mathrm{d}\widetilde{\boldsymbol{x}}}{\mathrm{d}t}=\boldsymbol{A}\widetilde{\boldsymbol{x}}+\widetilde{\boldsymbol{g}}(\boldsymbol{x}^*,\widetilde{\boldsymbol{x}}), \tag{3.1}$$

where

$$\widetilde{\boldsymbol{g}}(\boldsymbol{x}^*,\widetilde{\boldsymbol{x}})=\begin{pmatrix} 0\\ 0\\ \dfrac{-h(v_1^*-v_2^*+\widetilde{v}_1-\widetilde{v}_2)+h(v_1^*-v_2^*)}{m_f+m_a}\\ \dfrac{h(v_1^*-v_2^*+\widetilde{v}_1-\widetilde{v}_2)-h(v_1^*-v_2^*)}{m_v}\end{pmatrix}.$$

Here, $h(w)=c|w|^{\alpha}w$.

By (2.9), the total derivative of V along the orbit of system (3.1) is

$$\frac{\mathrm{d}V}{\mathrm{d}t}(\widetilde{\boldsymbol{x}}) = -C_a\widetilde{v}_1^2 - (\widetilde{v}_1 - \widetilde{v}_2)(h(v_1^* - v_2^* + \widetilde{v}_1 - \widetilde{v}_2) - h(v_1^* - v_2^*)). \tag{3.2}$$

Since h is strictly increasing on $\mathbb{R}$, we have $(a-b)\,(h(a+b) - h(b)) \geq 0$ for all $a, b \in \mathbb{R}$, with equality if and only if $a = 0$. Consequently,

$$(\widetilde{v}_1 - \widetilde{v}_2)(h(v_1^* - v_2^* + \widetilde{v}_1 - \widetilde{v}_2) - h(v_1^* - v_2^*)) \geq 0,$$

and the equality holds if and only if $\widetilde{v}_1 - \widetilde{v}_2 = 0$. Thus, along any orbit, $\dfrac{\mathrm{d}V}{\mathrm{d}t}(\widetilde{\boldsymbol{x}}(t)) \leq 0$.

Denote

$$D = \{\widetilde{\boldsymbol{x}} = (\widetilde{z}_1, \widetilde{z}_2, \widetilde{v}_1, \widetilde{v}_2)^{\mathrm{T}} \mid \widetilde{v}_1 = \widetilde{v}_2 = 0\}, \tag{3.3}$$

then $\left.\dfrac{\mathrm{d}V}{\mathrm{d}t}\right|_{\widetilde{\boldsymbol{x}}} = 0$ holds along the orbit at $\widetilde{\boldsymbol{x}}$ if and only if $\widetilde{\boldsymbol{x}} \in D$.

Next, we seek the largest invariant set within D. The orbit remaining in D satisfies

$$\widetilde{v}_1 = \widetilde{v}_2 = 0, \tag{3.4}$$

$$\frac{\mathrm{d}\widetilde{v}_1}{\mathrm{d}t} = \frac{\mathrm{d}\widetilde{v}_2}{\mathrm{d}t} = 0. \tag{3.5}$$

Substituting (3.4)–(3.5) into system (3.1), we get $\widetilde{z}_1 = \widetilde{z}_2 = 0$. Hence, the largest invariant set in D is $M = \{\mathbf{0}\}$.

Since $V(\widetilde{\boldsymbol{x}}(t))$ is positive definite and monotonically decreasing along any orbit, there exists a constant $a \geq 0$, which depends on the orbit, such that

$$\lim_{t\to+\infty} V(\widetilde{\boldsymbol{x}}(t)) = a \geq 0.$$

For any given $r > 0$, if the initial data satisfy $V(\widetilde{\boldsymbol{x}}(0)) \leq r$, then the forward orbit is contained within $P_r = \{\widetilde{\boldsymbol{x}} \in \mathbb{R}^4 \mid V(\widetilde{\boldsymbol{x}}) \leq r\}$. Since P_r is bounded, the forward orbit $\{\widetilde{\boldsymbol{x}}(t) \mid t \geq 0\} \subset P_r$ is also bounded. Although system (3.1) is non-autonomous, it is T-periodic in t through the term $v_1^* - v_2^*$; the argument below is therefore the invariance principle for periodic systems, in which the shift by one period plays the role of the discrete dynamical system. Thus the ω-limit set $L^+ \subset P_r$ is non-empty and invariant under this period-T shift. By the Bolzano-Weierstrass theorem, there exists a sequence $t_n = k_nT \to +\infty$ such that

$$\lim_{n\to+\infty} \widetilde{\boldsymbol{x}}(t_n) = \boldsymbol{p} \in L^+,$$

which leads to

$$V(\boldsymbol{p}) = \lim_{n\to+\infty} V(\widetilde{\boldsymbol{x}}(t_n)) = a.$$

Moreover, along the entire orbit Γ starting from $\boldsymbol{p}$, $V|_\Gamma = a$. Hence, this orbit lies in the largest invariant set M. Therefore, for any initial data, the Cauchy solution to system (3.1) converges globally asymptotically to $\mathbf{0}$. □

4 Uniqueness of T-Periodic Solution

Theorem 3 The T-periodic solution to system (1.3) is unique.

Proof By contradiction. Suppose that system (1.3) admits two distinct T-periodic solutions $\boldsymbol{x} = (z_1, z_2, v_1, v_2)^{\mathrm{T}}$ and $\boldsymbol{x}^* = (z_1^*, z_2^*, v_1^*, v_2^*)^{\mathrm{T}}$. If $z_1 \equiv z_1^*$ and $z_2 \equiv z_2^*$, then $v_1 = \dot{z}_1 \equiv \dot{z}_1^* = v_1^*$ and $v_2 \equiv v_2^*$, contradicting the assumption that the two solutions are distinct; hence there exists $t_0 \in [0, T]$ such that $|z_1(t_0) - z_1^*(t_0)| + |z_2(t_0) - z_2^*(t_0)| > 0$. Taking a sequence $t_k = t_0 + kT$ and using the T-periodicity, we have

$$|z_1(t_k) - z_1^*(t_k)| + |z_2(t_k) - z_2^*(t_k)| = |z_1(t_0) - z_1^*(t_0)| + |z_2(t_0) - z_2^*(t_0)| > 0. \tag{4.1}$$

On the other hand, by Theorem 2,

$$\lim_{k \to +\infty} |z_1(t_k) - z_1^*(t_k)| + |z_2(t_k) - z_2^*(t_k)| = 0, \tag{4.2}$$

which leads to a contradiction. Therefore, the T-periodic solution to system (1.3) is unique. □

5 Numerical Simulations

The system (1.3) is integrated numerically in the time domain over $[0, 50T]$ using the MATLAB `ode45` solver, which is based on the Runge-Kutta method. The script used for this integration, together with the hydrodynamic data files it reads, is provided as Supplementary Material (Online Resource 1), so that all results reported in this section can be reproduced by running it. The following parameter values are used in numerical simulations [3]: the mass of the floater $m_f = 206,089$ kg; the mass of the oscillator $m_v = 402,517$ kg; the radius of the floater base $r = 4$ m; the stiffness of the spring $k_s = 244,336$ N/m; the scaling coefficient of the power-law nonlinear damper $c = 1,560,000$ kg $\cdot$ m$^{-1/2}$ $\cdot$ s$^{-1/2}$; the power-law exponent $\alpha = 0.5$; the density of seawater $\rho = 1,025$ kg/m^3; the gravitational acceleration $g = 9.8$ m/s^2; the hydrostatic restoring force coefficient $k_f = \rho g \pi r^2 \approx 504,916.8$ N/m; the angular frequency of the wave excitation force $\omega = 0.7791$ rad/s; the period of the wave excitation force $T = \dfrac{2\pi}{\omega} \approx 8.0645$ s; the incident wave height $H = 2.5$ m; the added mass of seawater $m_a = 132,012.2$ kg; the wave excitation force amplitude per unit wave height $f_{e0} = 323,559.7$ N/m; the total wave excitation force $f_e = H \cdot f_{e0} = 808,899.4$ N; the radiation damping coefficient $C_a = 25,576.4$ N $\cdot$ s/m.

The initial data are chosen as

$$z_1(0) = 0 \text{ m}, \quad z_2(0) = 0 \text{ m}, \quad v_1(0) = 0 \text{ m/s}, \quad v_2(0) = 0 \text{ m/s}. \tag{5.1}$$

Fig. 3 shows the dynamics of z_1 and z_2. From Fig. 3, we can see that the frequencies of z_1 and z_2 are nearly identical. The last ten intervals between the adjacent wave peaks are all around 8.0645 s, which coincides with the period of the wave excitation force T.

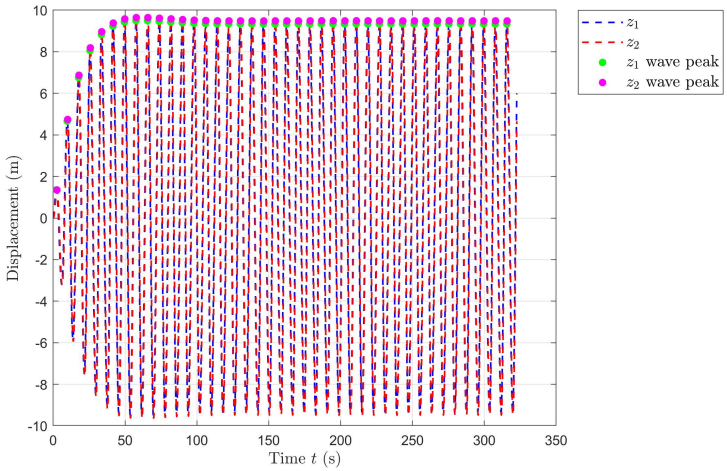


Fig. 3 The response curves of z_1 and z_2

Fig. 4 shows the variation of peak time intervals $(t_{k+1} - t_k)$. Within the first 3 periods, the peak intervals for both z_1 and z_2 exhibit intense fluctuations. After 3 periods, peak time intervals slightly oscillate around period T. This indicates that the peak intervals gradually reach the excitation period.

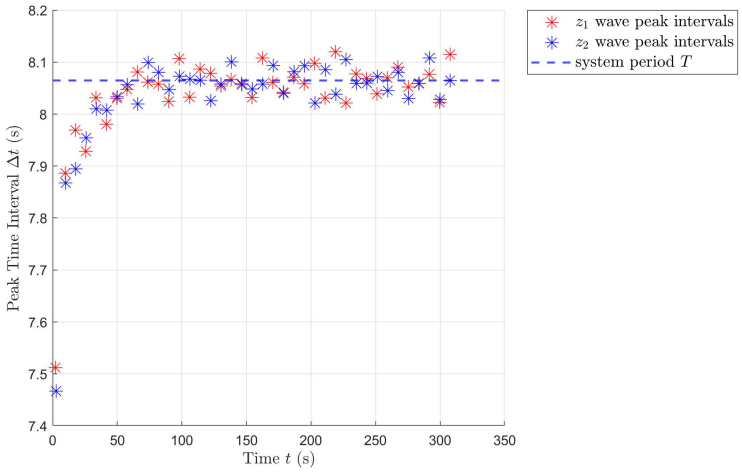
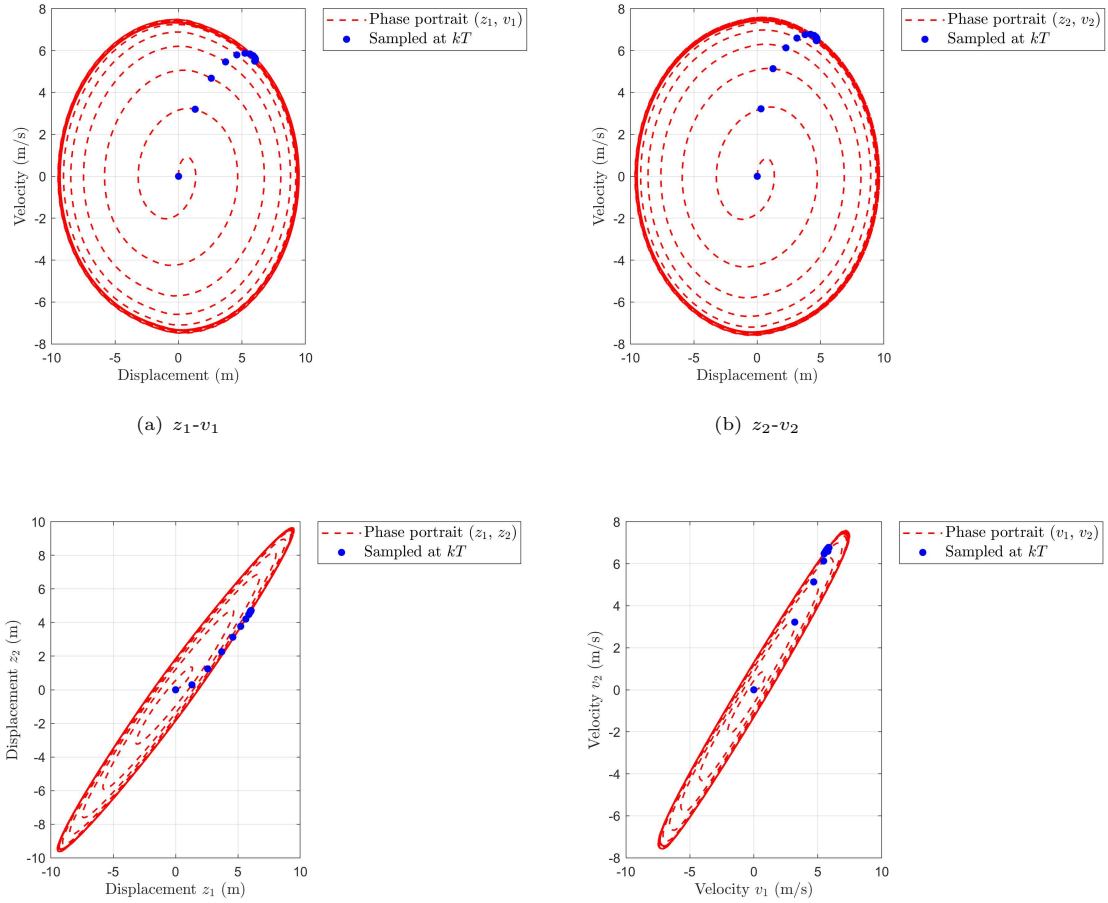


Fig. 4 The variation of peak time interval with time

Fig. 5 shows the orbit projecting onto the phase planes z_1-v_1, z_2-v_2, z_1-z_2, and v_1-v_2 (Fig. 5 (a)–(d)), respectively. The orbit in each phase plane approaches a limit cycle, and the phase points at integer periods converge to a single point.



(a) z_1-v_1 (b) z_2-v_2

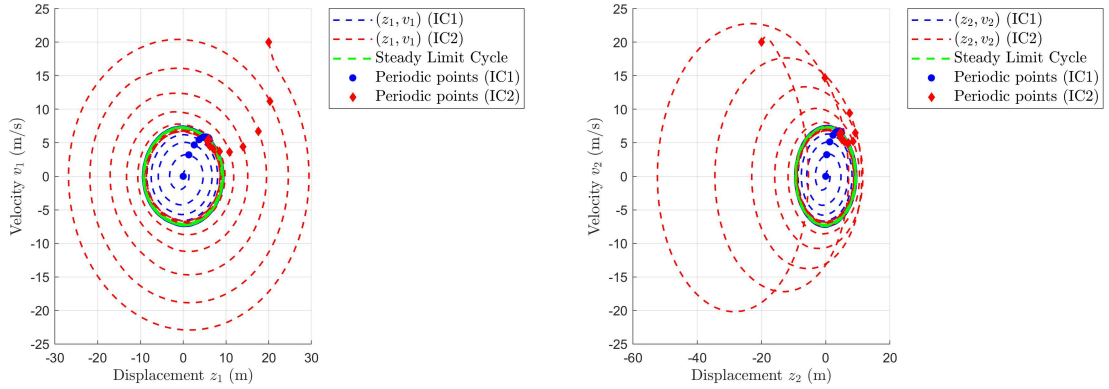
(c) z_1-z_2 (d) v_1-v_2

Fig. 5 Phase plane projections of the solution orbit

In order to validate the global attractivity, we consider the solutions to system (1.3) with two different initial data given by (5.1) and

$$z_1(0) = 20 \text{ m}, \quad z_2(0) = 20 \text{ m}, \quad v_1(0) = -20 \text{ m/s}, \quad v_2(0) = 20 \text{ m/s}. \tag{5.2}$$

Fig. 6 shows the orbits projecting onto the z_1-v_1 phase plane (Fig. 6 (a)) and the z_2-v_2 phase plane (Fig. 6 (b)). In Fig. 6 (a) and Fig. 6 (b), both orbits converge to the same limit cycle, and their phase points at integer periods converge to the same point.



(a) z_1-v_1 (b) z_2-v_2

Fig. 6 Projection of the orbits for different initial data over $[0, 50T]$

Fig. 7 shows the dynamics of the differences between each component of the solutions corresponding to initial data (5.1) and (5.2) (Fig. 7(a)–(d)). The differences of all components rapidly converge to 0, which confirms the uniqueness and global attractivity of the T-periodic solution.

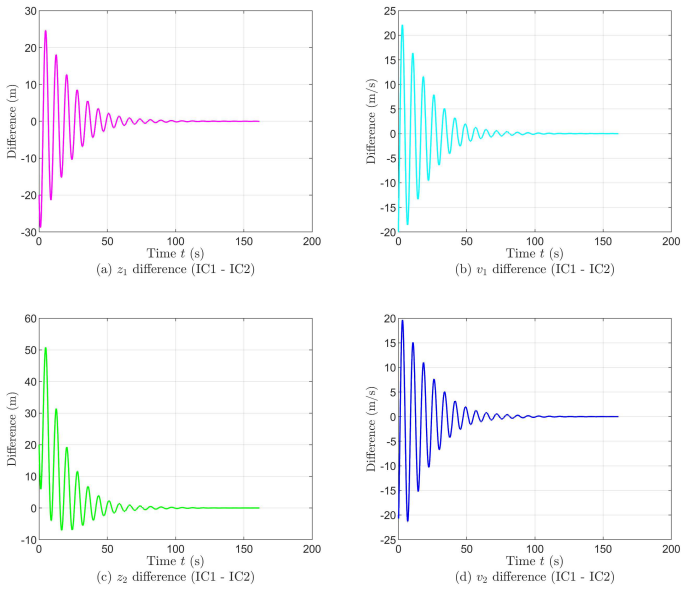


Fig. 7 Differences of solutions under different initial data

6 Conclusions

In this paper, we study the dynamics of a catamaran-type WEC equipped with a nonlinear damper under periodic wave excitation. By using coincidence degree theory, we rigorously prove the existence, uniqueness, and global attractivity of the T-periodic solution to the system. Furthermore, numerical simulations successfully validate the theoretical results.

We will attempt to estimate the convergence rate at which general Cauchy solutions converge to the periodic solution from an analytical perspective. Such estimates are

essential for characterizing the transient dynamics and global convergence properties of damped periodically driven systems, with direct implications for evaluating how quickly a WEC device reaches its steady energy-harvesting state from general initial conditions.

Furthermore, we will employ semi-analytical techniques to obtain numerical periodic solutions for concrete systems, and subsequently analyze the variation of the mean energy absorption rate with respect to system parameters.

Statements and Declarations

Funding The authors did not receive support from any organization for the submitted work.

Competing interests The authors have no relevant financial or non-financial interests to disclose.

Author contributions Xinhang Li carried out the theoretical analysis and the numerical simulations, prepared all figures and drafted the manuscript. Zhijie Cai proposed the research problem, verified the correctness of the theorem proofs, guided and arranged the numerical experiments, and revised the manuscript in several rounds. Both authors read and approved the final manuscript.

Data availability The physical parameters and hydrodynamic data used in this study are taken from the cited literature; no experimental datasets were generated. All data supporting the findings are available within the paper and its Supplementary Information (Online Resource 1), which also contains the data workbook `WEC_Data.xlsx`, or from the corresponding author on reasonable request.

Code availability The MATLAB script `WECFullCode.m` provided in the Supplementary Information (Online Resource 1) was written by the authors themselves: it implements the numerical integration of the governing equations and generates all numerical results and all figures reported in this paper. The hydrodynamic data workbook it reads (`WEC_Data.xlsx`) and a `README.txt` describing how to run the script are provided together with it. MATLAB R2019a or later is required, and no external toolbox is required.

References

[1] Manan Jariwala, A., Kumar Dash, S., Sahu, U.K., Mohan, H.M.: Performance optimization techniques on point absorber and oscillating water column wave energy converter: A comprehensive review. IEEE Access **13**, 14743–14759 (2025)

[2] Falnes, J., Kurniawan, A.: Ocean Waves and Oscillating Systems: Linear Interactions Including Wave-energy Extraction vol. 8, pp. 121–195. Cambridge university press, Cambridge (2020)

[3] Al Shami, E., Wang, Z., Wang, X.: Non-linear dynamic simulations of two-body wave energy converters via identification of viscous drag coefficients of different shapes of the submerged body based on numerical wave tank cfd simulation. Renewable Energy **179**, 983–997 (2021)

[4] Zhang, Y., Zhao, Y., Sun, W., Li, J.: Ocean wave energy converters: Technical principle, device realization, and performance evaluation. Renewable and Sustainable Energy Reviews **141**, 110764 (2021)

[5] Reguero, B., Losada, I., Méndez, F.: A global wave power resource and its seasonal, interannual and long-term variability. Applied Energy **148**, 366–380 (2015)

[6] Li, D., Dong, X., Li, Y., Huang, H., Shi, H.: Hydrodynamic performance and power absorption of a coaxial double-buoy wave energy converter. China Ocean Engineering **37**(3), 378–392 (2023)

[7] Amini, E., Asadi, R., Golbaz, D., Nasiri, M., Naeeni, S.T.O., Majidi Nezhad, M., Piras, G., Neshat, M.: Comparative study of oscillating surge wave energy converter performance: A case study for southern coasts of the caspian sea. Sustainability **13**(19), 10932 (2021)

[8] Guo, B., Wang, T., Jin, S., Duan, S., Yang, K., Zhao, Y.: A review of point absorber wave energy converters. Journal of Marine Science and Engineering **10**(10), 1534 (2022)

[9] Zhang, W., Zhou, Y., Xiaoguo, Z.: Power take-off mechanism analysis of oscillating-buoy wave energy converter. Journal of Vibration and Shock **39**(11), 38–44 (2020)

[10] Trueworthy, A., DuPont, B.: The wave energy converter design process: Methods applied in industry and shortcomings of current practices. Journal of Marine Science and Engineering **8**(11), 932 (2020)

[11] Li, D., Sharma, S., Borthwick, A.G., Huang, H., Dong, X., Li, Y., Shi, H.: Experimental study of a floating two-body wave energy converter. Renewable Energy **218**, 119351 (2023)

[12] Tan, J., Coe, R.G., Lavidas, G.: Benchmark of numerical modeling approaches on the systematic performance evaluation of wave energy converters. Applied Ocean Research **162**, 104725 (2025)

[13] Armesto, J.A., Guanche, R., Jesus, F.d., Iturrioz, A., Losada, I.J.: Comparative analysis of the methods to compute the radiation term in cummins' equation. Journal of Ocean Engineering and Marine Energy **1**(4), 377–393 (2015)

[14] Demonte Gonzalez, T., Parker, G.G., Anderlini, E., Weaver, W.W.: Sliding mode control of a nonlinear wave energy converter model. Journal of Marine Science and Engineering **9**(9), 951 (2021)

[15] Lelkes, J., Davidson, J., Kalmár-Nagy, T.: Modelling of parametric resonance for heaving buoys with position-varying waterplane area. Journal of Marine Science and Engineering **9**(11), 1162 (2021)

[16] Holappa, K., Falzarano, J.: Application of extended state space to nonlinear ship rolling. Ocean Engineering **26**(3), 227–240 (1998)

[17] Qin, J., Zhang, Z., Song, X., Huang, S., Liu, Y., Xue, G.: Design and performance evaluation of an enclosed inertial wave energy converter with a nonlinear stiffness mechanism. Journal of Marine Science and Engineering **12**(1), 191 (2024)

[18] Gu, X., Niu, Y., Zheng, Y., He, P., Chen, Q.: A study on multi-degree-of-freedom coupled hydrodynamic characteristics of a novel two-body wave energy converter. Journal of Vibration and Shock **43**(4), 207–214 (2024)

[19] Wan, Q., Li, Z., Zhang, C., Jin, Y.: The maximum output power of a wave energy conversion device under heave motion and study on the matching of optimal damping. In: Fifth International Conference on Mechanical Engineering and Materials (ICMEM 2024), vol. 13547, pp. 649–657 (2025). SPIE

[20] Li, D., Dong, X., Borthwick, A.G.L., Sharma, S., Wang, T., Huang, H., Shi, H.: Two-buoy and single-buoy floating wave energy converters: A numerical comparison. Energy **296**, 131219 (2024)

[21] Lewis, A.: Enhanced method for forced strongly nonlinear two-degree-of-freedom nonlinear systems using an integro-differential equation approach: Ap lewis. Nonlinear Dynamics **113**(16), 20767–20791 (2025)

[22] Razzak, M., Alam, M., Sharif, M.: Modified multiple time scale method for solving strongly nonlinear damped forced vibration systems. Results in physics **8**, 231–238 (2018)

[23] Mawhin, J.: Topological degree and boundary value problems for nonlinear differential equations. In: Topological Methods for Ordinary Differential Equations, pp. 74–142. Springer, Italy (2006)

[24] Khasawneh, M.A., Daqaq, M.F.: Response behavior of bi-stable point wave energy absorbers under harmonic wave excitations. Nonlinear Dynamics **109**(2), 371–391 (2022)

[25] Guo, D.: Nonlinear Functional Analysis. Shandong Science and Technology Press, Jinan (2001)

[26] Madsen, I.H., Tornehave, J.: From Calculus to Cohomology: De Rham Cohomology and Characteristic Classes. Cambridge university press, Denmark (1997)

[27] Adams, R.A., Fournier, J.J.: Sobolev Spaces vol. 140. Elsevier, Vancouver, Canada (2003)

Supplementary Files

This is a list of supplementary files associated with this preprint. Click to download.

- ESM1.zip